

Numerical deflation of beach balls with various Poisson's ratios: from sphere to bowl's shape

March 15, 2019

Abstract

We present a numerical study of the shape taken by a spherical elastic surface when the volume it encloses is decreased. For the range of 2D parameters where such surface may modelize a thin shell of an isotropic elastic material, the mode of deformation that develops a single depression is investigated in detail. It first occurs via buckling from sphere toward an axisymmetric dimple, followed by a second buckling where the depression loses its axisymmetry, by folding along portions of meridians. We could exhibit unifying master curves for the relative volume variation at which first and second buckling occur, and clarify the role of the Poisson's ratio. After the second buckling, the number of folds and inner pressure are investigated, allowing to infer shell features from mere observation and/or knowledge of external constraints.

1 Introduction

Let's consider a thin shell of an elastic isotropic material, such as a beach ball, and deflate it. What shape will it take ?

The interest of this question is not restricted to garrulous familial shores : fundamental and applied physics nowadays presents legions of easily deformable soft objects, and knowing what governs their shapes gives the powerful possibility of inferring mechanical properties from simple observations, without contact. Among these deformable objects, an increasing number derives from spherical symmetry, that is omnipresent at scales where surface effects overcome volume forces such as gravity. The numerical study presented in this paper discusses the shapes taken by spherical thin shells of isotropic materials when their inner volume is decreased by an important amount. Such a systematic and quantitative study will help deciphering conformations observed in *e.g.* Soft Matter (colloidal shells, solid-phase vesicles), galenics (encapsulation), microfluidics (microtanks) or medicine (ultrasound contrast agents), under the action of an external pressure or other possibly isotropic fields such as concentration in evaporation/dissolution phenomena.

When an elastic spherical shell has its inner volume lowered, it first deforms through in-plane compression that respects the spherical symmetry. Then it undergoes a symmetry breaking in order to relax a high stretch energy into much lower bending energy, by reversion of a spherical cap (creation of an axisymmetric depression, or "dimple"). The onset of this sudden transition, or buckling, under external pressure was studied long ago by Pogorelov and Landau[1, 2]. They showed that the dimple should nucleate over a critical outside/inside pressure difference $\Delta P_{Landau} = Y_{3D} \left(\frac{d}{R}\right)^2$, where d is the shell thickness, R its radius and Y_{3D} the Young modulus of the material that makes it up. Its edge (or "rim") has a transversal extension \sqrt{dR} . One of the key of their calculation being the assumption that buckling occurs for dimples such that maximum deflection is of order d , spherical geometry imposes then that \sqrt{dR} is also the radius of the dimples that forms.

Results focusing on deformations through further deflation are, mainly, more recent. Experimental [3, 4, 5, 6, 7, 8] and numerical [4, 9] deflations showed shapes holding several dimples, also called “multiple indentation”. These conformations compete with observations of shapes holding a single depression [5, 7], possibly losing axisymmetry [10] or exhibiting folding perpendicularly to the rim [11, 6]. Similar shapes are observed in shells under a point load [12, 13] or pressed against a wall [14, 13]. Secondary buckling by folding of the single depression, also called “polygonal indentation”, under isotropic constraint was numerically retrieved with a surface model [11, 9]. Thin shells with a single depression, either axisymmetric or polygonal, appears to present a conformation of lower energy than the metastable multiple indentation [11, 9, 15]. In the case of an axisymmetric dimple, this can be easily understood since elastic energy mainly concentrates in dimple edges as bending energy, with an energy per edge length that weakly varies with dimple size. Hence dimples coalescence lowers the total elastic energy [16]. Nevertheless, more than one dimple may nucleate if the deflation is rapid enough, leading to metastable multi-indented shapes [15]. The term “rapid” is to be taken on a wide acception here. Experimentally, it may corresponds to situations where dissipation (due to material viscosity or to fluid flows accompanying the deformation) prevents from dimple growth, which favors secondary nucleation once ΔP_{Landau} is reached, and where subsequent kinetics prevents from thermally activated coalescence between adjacent dimples. Numerically, minimization may reproduce such metastable situations, such as in [9] or [15], since (i) important volume increments favors creation of extra dimples, by making difficult to find the cooperative displacement of vertices that corresponds to rim rolling in dimple growth (ii) depending on the way curvatures are calculated, energy barriers that prevents from dimple coalescence may be overcome or not. For “slow” deflations, a single dimple can appear and grow, or freshly nucleated dimples may coalesce into a single one. Such “slow” deflation provides an axisymmetric bowl-like shape, that may undergo under further deflation a transition toward a non-axisymmetric depression, *i.e.* polygonal indentation [11].

We present here a systematic numerical study of such “slow” deflations leading to shapes with a single depression. In this purpose, we used a surface model taking into account recent developments, presented in section 2. We clearly expose the correspondence between 2D parameters of the model surface, and 3D properties of the real object of nonzero thickness, expliciting the role of the different significative parameters. Particular emphasis is put on a parameter often underconsidered: the Poisson’s ratio.

The whole study allows to determine parameters of importance for the transitions sphere \rightarrow axisymmetric bowl (section 3) and axisymmetric bowl \rightarrow polygonal indentation (section 4), for the detailed shape in polygonal indentation, and for inner pressure. Furthermore, we took particular care to provide empirical dependence laws for practical use.

2 Surface model

Surface model, where out-of-plane and in-plane deformations are formally uncoupled, is for long considered as valid to describe the deformation of thin sheets (plates or shells) [2, 17]. For thin sheets without spontaneous curvature (*i.e.* an elementary surface portion of the sheet, freed from constraints exerted by surrounding material, remains flat at equilibrium), the energies per surface unit that are to be considered in this surface model are of two kinds. On the one hand, a curvature term that can express $\frac{1}{2}\kappa c^2 + \bar{\kappa}g$ [18, 2], where $c = \frac{1}{R_1} + \frac{1}{R_2}$ and $g = \frac{1}{R_1} \times \frac{1}{R_2}$ are respectively the mean and Gaussian curvatures (R_1 and R_2 being the local principal curvature radii), and κ and $\bar{\kappa}$ are respectively the mean and Gaussian curvature constants [19]. The other term may be written, in a Hookean linear model: $\frac{1}{2}\epsilon_{ij}K_{ijkl}\epsilon_{kl}$, where ϵ_{ij} and K_{ijkl} respectively represent the two-dimensional strain and elasticity tensors for in-plane deformations. For an homogeneous and isotropic surface, the nonzero terms of the two-dimensional elasticity tensor are $K_{xxxx} = K_{yyyy} = \frac{Y_{2D}}{1-\nu_{2D}^2}$, $K_{xxyy} = K_{yyxx} = \frac{\nu_{2D}Y_{2D}}{1-\nu_{2D}^2}$ and $K_{xyxy} = K_{yxxy} = \frac{Y_{2D}}{1+\nu_{2D}}$, with Y_{2D} the two-dimensional Young modulus and ν_{2D} the two-dimensional Poisson ratio, which is comprized between

-1 and 1 [2]. This in-plane elasticity term can be rewritten as $\frac{Y_{2D}}{2(1+\nu_{2D})} \left[\text{Tr}(\epsilon^2) + \frac{\nu_{2D}(\text{Tr}\epsilon)^2}{1-\nu_{2D}} \right]$ for the sake of concision.

In a linear approximation, these 2D parameters are related to the 3D features of the plate (Young modulus Y_{3D} , Poisson's ratio ν_{3D} , thickness d) with zero boundary tangential constraints [2] through the relations (explicated *e.g.* in [14] or [20]):

$$\nu_{2D} = \nu_{3D} = \nu \quad (1)$$

$$Y_{2D} = Y_{3D}d \quad (2)$$

$$\kappa = \frac{Y_{3D}}{12(1-\nu^2)} d^3 \quad (3)$$

$$\bar{\kappa} = (\nu - 1) \kappa = -\frac{Y_{3D}}{12(1+\nu)} d^3 \quad (4)$$

Since for bulk materials the maximum value of ν_{3D} is $\frac{1}{2}$ for thermodynamic reasons [2], one can constat that the range of 2D Poisson's ratio that can describe a thin plate of an isotropic material is limited to a maximum value of $\frac{1}{2}$. In other terms, even a thin plate of an incompressible isotropic material cannot behave as an incompressible surface (where $\nu_{2D} = 1$), thanks to the possibility of having its thickness varied. On the other limit, Poisson's ratio can reach -1 as a lower value, but negative values correspond to less common "auxetic" materials.

Conversely, the thickness of the plate can express through 2D parameters with:

$$d = \sqrt{12(1-\nu^2) \frac{\kappa}{Y_{2D}}} \quad (5)$$

For describing constraints-free thin shells, a spontaneous curvature [18] has to be introduced, that allows elastic energy to be minimum in the initial conformation. It was recently shown how to take the local spontaneous curvature (*i.e.* the curvature taken by any isolated surface element) into account in the gaussian curvature term[21], in order to minimize the free energy per surface unit. For an unstrained spherical surface of radius R , the total curvature energy to be considered is:

$$E_{curvature} = \int_{shell\ surface} \left[\frac{1}{2} \kappa \left(c - \frac{2}{R} \right)^2 + \bar{\kappa} \left(\frac{1}{R_1} - \frac{1}{R} \right) \left(\frac{1}{R_2} - \frac{1}{R} \right) \right] dS \quad (6)$$

This expression is slightly different from what is obtained by simply replacing spontaneous curvature by $\frac{2}{R}$ in Helfrich's energy, like what was done *e.g.* in [11], hence we will quantitatively discuss, in the results, differences induced by the use of this expression. Following [21], the three contributions (in-plane, mean curvature and gaussian energy) can be rewritten as

$$E_{elastic} = cst + \int_{shell\ surface} \left[\frac{1}{2} \kappa (c - c_0^*)^2 + \frac{1}{2} \epsilon_{ij} K_{ijkl} \epsilon_{kl} + \gamma_{eff} \right] dS \quad (7)$$

with $c_0^* = \frac{1+\nu}{R}$ being the effective spontaneous curvature, and $\gamma_{eff} = \frac{(1-\nu^2)\kappa}{2R^2}$ an effective surface tension.

Size influence will be considered by using the adimensionalized Föppl-von Kármán number[22] $\gamma = \frac{Y_{2D}R^2}{\kappa}$, that mostly balances in-plane and out-of plane deformations. An elastic surface with the energy given in equation (7) can effectively describe a thin shell of isotropic material if $\frac{12(1-\nu^2)}{\gamma} \ll 1$, in addition to the condition $\nu_{2D} \leq \frac{1}{2}$. In this range, γ roughly scales like $\left(\frac{R}{d}\right)^2$. Out of this range, such a surface model

does not correspond to any thin shell of an isotropic material ; it can nevertheless describe different types of objects, *e.g.* thin shells of non isotropic materials[15].

Numerical experiments are performed by minimizing the elastic energy as expressed in equation (7) for different inner volumes, with the free software Surface Evolver[24]. A whole in-silico deflation experiment (from $V_{init} = \frac{4}{3}\pi R^3$ to around $0.2 \times V_{init}$) is realized through succession of different equilibrium states, these latter found according the process described in [11], and calculated successively for inner volumes decreased by steps of at maximum 2% of the initial volume (steps amplitude is reduced in some situations in order to avoid the nucleation of secondary dimples).

3 First-order transition toward axisymmetric depression

Deflation of a spherical elastic surface, at imposed either volume or external pressure, causes an abrupt buckling from the spherical conformation. The mechanism has been quite recently studied in detail by Knoche *et al*[23], with study of various metastability branches. In our simulations, designed to not to be stuck in multi-indentation conformations of higher energy, or other less stable, this first buckling leads to a single axisymmetric dimple. Our purpose here is to provide a general description of buckling features at controlled volume, for the range of adimensional parameters that scans the generality of thin shells of isotropic material. The dimensionless parameters involved in the shape are the relative volume variation $\frac{V_{init}-V}{V_{init}} = \frac{\Delta V}{V}$, the Föppl-von Karman parameter γ and the Poisson's ratio ν . We refer by $(\frac{\Delta V}{V})_{buck\ 1}$ to the relative volume variation at which buckling from the spherical conformation occurs ; simulations showed that $(\frac{\Delta V}{V})_{buck\ 1}$ varies as a power-law of γ with an exponent near from $-\frac{1}{2}$ (linear regression on the logarithms provide exponents between -0.50 and -0.51 for ν varying from -0.5 to 0.5, with correlation coefficients better than 0.999). In order to get an unified description, we thus searched the best coefficient b allowing a description of $(\frac{\Delta V}{V})_{buck\ 1}$ in $b \times \gamma^{-1/2}$ (least squares). The dependence of b with ν is shown figure 1; it clearly exhibits a linear behaviour with $(1 - \nu)$. Extending our purpose out of the range of 2D parameters that effectively can describe a thin shell of isotropic material, we may remark that extrapolation to $\nu = 1$ shows expected vanishing of b : this limit corresponds to incompressible surfaces (2D compressibility modulus may express as $\chi_{2D} = \frac{Y_{2D}}{2(1-\nu)}$), that will necessarily undergo a deformation with curvature even for the smallest volume decreases, since area variation is prohibited. At the opposite limit, for the most auxetic materials, increase of $(\frac{\Delta V}{V})_{buck\ 1}$ up to disappearance of sphere \rightarrow bowl buckling is expected when ν approaches -1, since χ_{2D} decreases and κ diverges, which makes curvature deformation prohibitive compared to in-plane compression. Hence b is expected to diverge when $\nu \rightarrow -1$, justifying the discrepancy from linear behaviour at $\nu = -0.8$. Far enough from this limit, numerical results suggests the existence of a phenomenological master curve :

$$\left(\frac{\Delta V}{V}\right)_{buck\ 1} = 6(1 - \nu)\gamma^{-\frac{1}{2}} = \sqrt{3} \left(\frac{1 - \nu}{1 + \nu}\right) \times \frac{d}{R} \quad (8)$$

This relation is compared to previous results obtained in [11] on figure 2. It shows that the modified form of curvature energy displayed in equation (6) leads increases the threshold of the first buckling by a slight amount (up to 20%) for the thinnest shells, but results are totally comparable for thicker shells.

We do not have for the moment a theoretical explanation for the fine role of ν in this first-order buckling, but figure 2 shows that this expression indeed provides a master curve accurate to describe a large range of shells. In terms of volume, the onset of buckling depends mainly on the relative thickness $\frac{d}{R}$, with only a weak influence of the Poisson's ratio. Since this latter ranges between 0 and $\frac{1}{2}$ for common materials (*i.e.* non auxetic, with $\nu \geq 0$), the prefactor of $\frac{d}{R}$ varies between $\sqrt{3}$ and 1, which is much less important than the range in $\frac{d}{R}$ that can be explored.

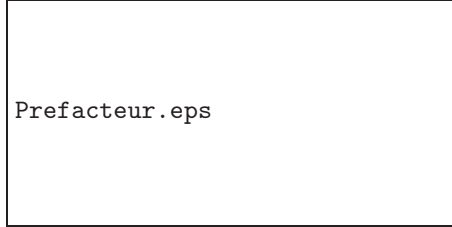


Figure 1: Optimal prefacteur b in the power-law $(\frac{\Delta V}{V})_{buck1} = b \times \gamma^{-1/2}$, with $\gamma = \frac{Y_{2D} R^2}{\kappa}$ and $(\frac{\Delta V}{V})_{buck1}$ the relative volume variation at the first buckling (sphere→bowl), for different Poisson's ratio ν . Dotted line: $b = 6(1 - \nu)$.

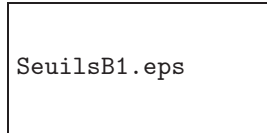


Figure 2: Relative volume variation $(\frac{\Delta V}{V})_{buck1}$ at the sphere→bowl buckling (lower and upper limit of the error bars are indicated respectively by upward and downward triangles). White: $\nu = 0.5$; light gray: $\nu = 0$; dark grey: $\nu = -0.5$; black: $\nu = -0.8$. Grey line: $(\frac{\Delta V}{V})_{buck1} = 6(1 - \nu) \gamma^{-\frac{1}{2}}$ (expressed through 3D parameters: $(\frac{\Delta V}{V})_{buck1} = \sqrt{3 \left(\frac{1-\nu}{1+\nu} \right) \times \frac{d}{R}}$). Dotted line: relation established in [11] for $\nu = 0.333$ (discussed in text). Illustrative inserts display deflated spherical surfaces at $\gamma = 4666$ and $\nu = -0.8$ (hence $\frac{d}{R} = 0.0304$), with relative volume variations respectively $\frac{\Delta V}{V} = 0.161$ (spherical) and 0.167 (buckled, section view, same scale).

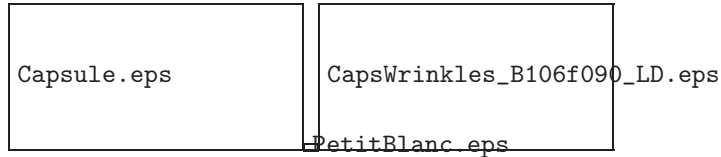


Figure 3: Left: schematisation of a spherical surface near complete deflation. Inner part of the rim endures a compressive stress in the direction indicated by the red double arrow. Relaxation of in-plane deformation occurs, for the thinnest shells, via undulation deformation, generating “wrinkles” all along the rim (examples schematized with blue interrupted lines). Length ℓ stands for lateral extension of the wrinkles. Right: simulation ($\gamma = 9.33 \cdot 10^3$ and $\nu = 0.5$ ($\frac{d}{R} = 0.0311$); $\frac{\Delta V}{V} = 0.562$). Maxima of undulation are stressed with blue interrupted lines ; circle locates the zone of high curvature that forms the apex of the s-cone.

We may notice that the $\gamma^{-1/2}$ dependence is quite near from the $\gamma^{-3/5}$ scaling expected from the cross-over between spherical compression energy and pure curvature energy in the description of the axisymmetric depression[11]. For the thickest shells, *i.e.* $\gamma \lesssim 30$, transition occurs not any more through sudden inversion of a spherical cap, but by slowly deforming into an ovoid shape, that flattens at the location of future depression under further deflation. We did not, here, specifically study this extreme behaviour.

4 Second-order transition toward polygonal depression

4.1 Location of the transition

In the axisymmetric bowl shape, global bending of the rim on the equator costs in-plane deformation: extension on the outer side of the rim, and compression on the inner one. For the thinnest shells, compressive stress parallel to the equator leads to a secondary buckling, where the inner side of the rim undulates to adapt to axial compression (fig. 3, left), forming “wrinkles” that deform the axisymmetric depression into a roughly polygonal shape (fig. 3, right). Such a conformation mainly involves curvature deformations, much less energetic than the compression energy of the spherical shape that quadratically increases with $\frac{\Delta V}{V}$ [14]. Fig. 4 shows how elastic energy dispatches in a typical numerical deflation. “Wrinkles” match with the rim through a zone of high curvature that has a folding role similar to what realizes the apex of d-cones [25, 26, 27], except that the surface is not developpable but spherical, hence the concept of “s-cones” proposed by Reis and Lazarus [28].

Secondary buckling from axisymmetric bowl shape to polygonal indentation, quite smooth, is harder to detect than the first one. We determined the range on the relative volume variation $(\frac{\Delta V}{V})_{buck 2}$ at which it occurs on the one hand by the maximum deflation before loss of axisymmetry, and on the other hand by the $\frac{\Delta V}{V}$ at which the rim presents convex zones under axial observation (as shown on lower part of Fig. 4, subfigure c). Figure 5 displays values of $(\frac{\Delta V}{V})_{buck 2}$ determined this way for different Poisson’s ratio, versus Föppl-von Kármán number . Here also the use of equation (6) for the energy slightly displaces the onset of buckling, but not by more than 20% on $(\frac{\Delta V}{V})_{buck 2}$. Data indicate a dependence in γ that does not show influence by ν ; linear regression on logarithms provides with a correlation coefficient of -0.98:

$$\left(\frac{\Delta V}{V}\right)_{buck 2} = 9267 \times \gamma^{-1.102} \quad (9)$$

[NB: plotting $\ln\left\{\left(\frac{\Delta V}{V}\right)_{buck 2}\right\}$ versus $\ln\left(\frac{d}{R}\right)$, as for the first buckling, increases data scattering, which results in a correlation coefficient of only -0.93]. Extrapolating this power-law up to $\frac{\Delta V}{V} = 1$ suggests

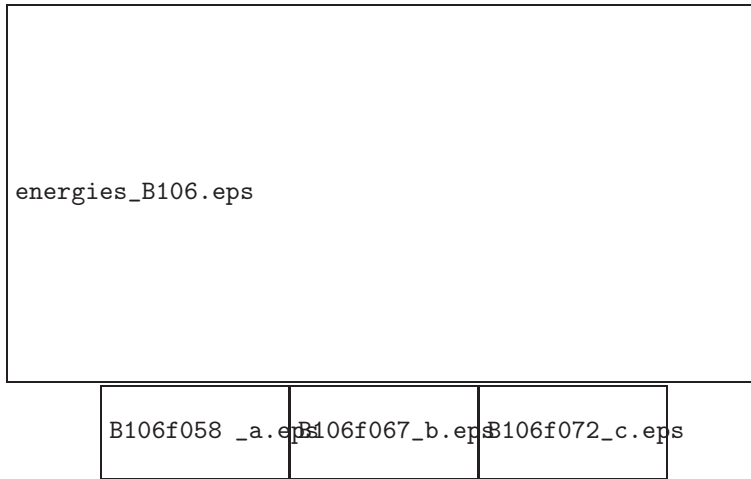


Figure 4: Deformation energies at different relative volume variations, adimensionalized by the curvature constant κ , for $\gamma = 9.33 \cdot 10^3$ and $\nu = 0.5$ ($\frac{d}{R} = 0.0311$). Interrupted line: Hookean in-plane deformation energy, linked to the second significative term of eq. (7), *i.e.* $\frac{1}{2}\epsilon_{ij}K_{ijkl}\epsilon_{kl}$. Grey continuous line: elastic energy linked to the first significative term : $\frac{1}{2}\kappa(c - c_0^*)^2$. This term does not vanish at $\frac{\Delta V}{V} = 0$ because $c_0^* \neq c_0$; in the total elastic energy, it is counterbalanced by the *cst* and the effective surface term expressed by γ_{eff} in equation (7). Effective surface energy (not represented here) varies at maximum by -0.33κ , and on an amplitude 0.03κ in the nonspherical conformations. Grey zone indicates the second transition from axisymmetric bowl shape to depression with inner wrinkles (“polygonal indentation”[9]), determined as explained in the text. First transition from sphere to axisymmetric bowl occurs through abrupt decrease of the in-plane deformation energy, at $\frac{\Delta V}{V} = 0.03$.

buck2.eps

Figure 5: Relative volume variation at which the axisymmetric depression becomes “polygonal”, versus $\sqrt{12}/\gamma$ (which is to be identified with d/R when $\nu = 0$). White: $\nu = 0.5$; light grey: $\nu = 0$; dark grey: $\nu = -0.5$; black: $\nu = -0.8$. Grey line: $(\frac{\Delta V}{V})_{buck2} = 9267 \times \gamma^{-1.102}$. Stripped zone roughly indicates spherical deformations, which exact location in this diagram depends on Poisson’s ratio ν . Dotted line: relation established in [11] for $\nu = 0.333$. Simulations indicating respectively the axisymmetric depression zone, and the polygonal depression zone, correspond to $\gamma = 3.22 \cdot 10^4$ and $\nu = 0.5$ ($\frac{d}{R} = 1.67 \cdot 10^{-2}$), with relative volume variations respectively $\frac{\Delta V}{V} = 0.065$ and $\frac{\Delta V}{V} = 0.737$.

that this secondary buckling does not happen, *i.e.* single indentation keeps its axisymmetry, above a threshold value $\gamma_{c,buck2} = 3979$. In tridimensional parameters, relation (10) expresses:

$$\left(\frac{\Delta V}{V}\right)_{buck2} = 38.7 \times \left(\frac{d/R}{\sqrt{1-\nu^2}}\right)^{2.204} \quad (10)$$

The dependence in ν , for non-auxetic materials, is even weaker than for the axisymmetric buckling since the prefactor varies at maximum by a factor 4/3. Relation (10) also implies that wrinkles are not expected when $d/R \gtrsim 0.059 \times \sqrt{1-\nu^2}$. A particular consequence is that in wrinkles prevention, a very auxetic material (with $\nu \rightarrow -1$) may help.

4.2 Characterisation of buckled shapes

For the thinnest shells that undergo polygonal indentation, the most conspicuous feature is the number W of wrinkles, or s-cones. Figure 6 shows the evolution of W for a typical deflation: first does W decrease while the freshly nucleated and still very flat depression hollows and enlarges, then it increases again. Data are quite scattered: there is a typical noise of order ± 1 on W , that has no observable correspondence in smooth energy curves (fig. 5). In order to decrease data scattering, we calculated $W_{deflated}$ as the average value of W between $\frac{\Delta V}{V} = 0.53$ and $\frac{\Delta V}{V} = 0.76$ (these values have been chosen in order to cover a significant range of relative volume variation before autocontact for all the simulations, that happens around $\frac{\Delta V}{V} \approx 0.9$). Values of $W_{deflated}$ are comparable with results from previous model, which did not take gaussian curvature into account, and indicates a scaling law in $\gamma^{-1/4}$ [11, 20]. With the model presented in paragraph 2, that deals with the nonzero spontaneous curvature even in the gaussian curvature term, we systematically studied the dependance of $W_{deflated}$ with γ and ν . As shown on figure 7, data are still compatible with a scaling in $\gamma^{-1/4}$, *i.e.* in $(\frac{d}{R})^{-1/2}$ with 3D parameters. This provides clues on the typical transversal size l of the s-cones (presented on figure 3, left). Since s-cones stand alongside one another on a length which is of the order of an equator (when the sphere is highly deflated), we can estimate l as $\frac{2\pi R}{W_{deflated}}$. Hence best fit of $W_{deflated}$ with dependence in $(\frac{d}{R})^{-1/2}$ (figure 7) rewrites:

$$l \approx 6.7 \sqrt{dR} \quad (11)$$

This shows that \sqrt{dR} scales not only for the rim width of the axisymmetric depression[2, 23], but also for s-cones size in polygonal depressions.

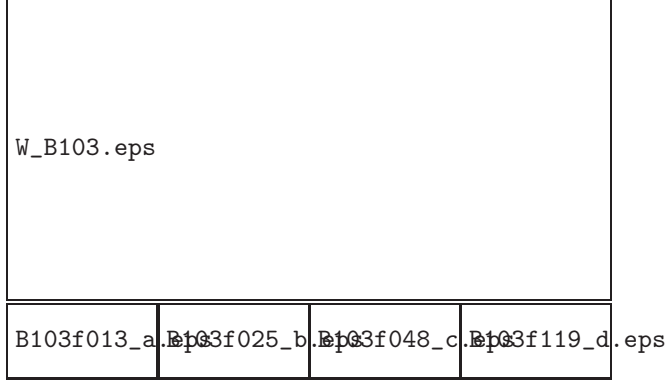


Figure 6: Number of wrinkles (s-cones) held by the single depression after the secondary buckling of figure 4. Poisson's ratio $\nu = 0.5$; Föppl-von Karman number $\gamma = 6.06 \cdot 10^4 (\frac{d}{R} = 0.0122)$. Lower part: conformations at points indicated on the main figure.

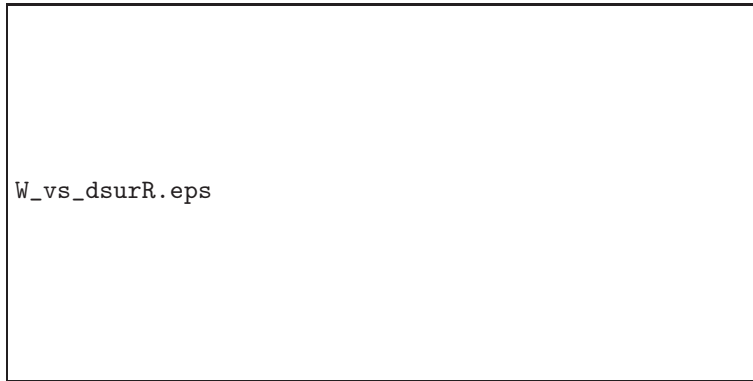


Figure 7: Number $W_{deflated}$ of wrinkles (s-cones) at the end of a numerical deflation (averaged between $\frac{\Delta V}{V} = 0.53$ and $\frac{\Delta V}{V} = 0.76$). Error bar are taken as the standard deviation on this range, with a minimum value of ± 0.5 . White: $\nu = 0.5$; light grey: $\nu = 0$; dark grey: $\nu = -0.5$; black: $\nu = -0.8$. Continuous line: $W_{deflated} = 0.940 \times (\frac{d}{R})^{-\frac{1}{2}}$.

PressionExample2.eps

Figure 8: Pressure difference $\Delta P = P_{ext} - P_{int}$ adimensionalized by $\Delta P_{Landau} = Y_{3D} \left(\frac{d}{R}\right)^2 = [12 Y_{2D} \kappa (1 - \nu^2)]^{1/2} / R^2$, as a function of the relative volume variation, for surfaces of similar Poisson's ratio $\nu = -0.5$. Dotted green: $\gamma = 1.17 \cdot 10^5$ ($\frac{d}{R} = 8.8 \cdot 10^{-3}$); blue: $\gamma = 6.07 \cdot 10^4$ ($\frac{d}{R} = 1.22 \cdot 10^{-2}$), interrupted orange: $\gamma = 3.22 \cdot 10^4$ ($\frac{d}{R} = 1.67 \cdot 10^{-3}$), magenta: $\gamma = 1.17 \cdot 10^4$ ($\frac{d}{R} = 2.31 \cdot 10^{-3}$), light blue: $\gamma = 9.33 \cdot 10^3$ ($\frac{d}{R} = 3.11 \cdot 10^{-2}$), parma: $\gamma = 4.67 \cdot 10^3$ ($\frac{d}{R} = 4.39 \cdot 10^{-2}$). Notice scale switch at $\frac{\Delta V}{V} = 0.2$. Points (corresponding each to a minimization) emphasizes two curves with typical behaviour: increasing (green curve), and plateauing (orange) .

ν	0.5	0	-0.5	-0.8
$\frac{\Delta P_{buck1}}{\Delta P_{Landau}}$	1 - 1.35	0.9 - 1.2	1.3 - 1.45	2.1 - 2.4

Table 1: Range of $\Delta P_{buck1}/\Delta P_{Landau}$ for γ between $4.67 \cdot 10^3$ and $2.33 \cdot 10^5$.

5 Pressure

As exposed previously, first buckling relaxes in-plane constraints, and as such lowers the inside/outside pressure difference $\Delta P = P_{ext} - P_{int}$. Figure 8 displays typical evolutions for pressure difference: first a linear increase followed by a drop at first buckling, after which pressure difference varies in a much lesser extent. Linear behaviour is expected before first buckling due to the relation between pressure and elastic energy $P_{ext} - P_{int} = \partial E_{elastic} / \partial (\Delta V)$ [20], and quadratic dependence of ΔP with $\Delta V = V_{init} - V$ (see *e.g.* [11]). One may constat that first buckling effectively occurs at a pressure difference of order ΔP_{Landau} (section 1). Taking into account the incertitude due to discrete volume increments, $\Delta P_{buckling1}/\Delta P_{Landau}$ is not affected by γ for a given Poisson's ratio (see *e.g.* figure 8), hence it does not depend on $\frac{d}{R}$, but more surprisingly it strongly depends on the Poisson's ratio (table 1), through a term that can vary up to twice. This indicates that buckling pressure is of the form:

$$\Delta P_{buckling1} = Y_{3D} \left(\frac{d}{R}\right)^2 \times function(\nu)$$

After the first buckling, we identified for the pressure difference two types of features on the range of parameters studied:

For $\frac{d}{R} > 0.014$, pressure difference ΔP presents the type of evolution calculated by [23], *i.e.* quasi-plateauing after buckling (variation of about 15% during the whole deflation, plus some occasional dispersion due to numerical procedure). Furthermore, an order relation is respected: at every volume step, the ratio $\frac{\Delta P}{\Delta P_{Landau}}$ weakly increases when γ decreases.

For the thinnest shells (in practice $\frac{d}{R} < 0.012$), $\frac{\Delta P}{\Delta P_{Landau}}$ regularly re-increases with deflation after the pressure drop, crossing successively the curves at smaller γ 's.

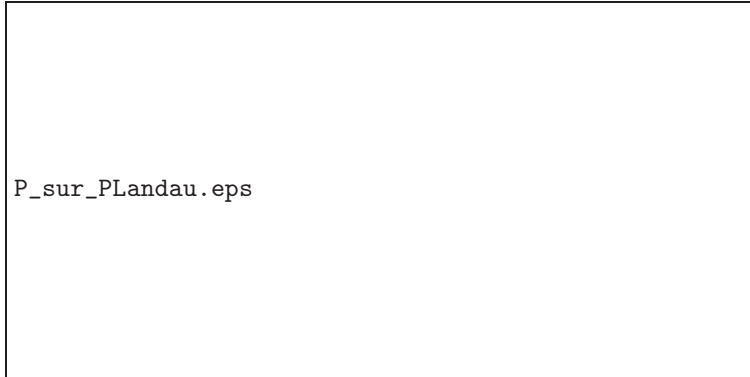


Figure 9: Minimum inside/outside pressure difference after buckling (cf figure 8), adimensionalized by Landau pressure, logarithmic representation. Black: $\nu = 0.5$; dark grey: $\nu = 0$; light grey: $\nu = -0.5$; white: $\nu = -0.8$. Interrupted line separates the two types of evolution of the pressure after the first buckling: increasing or plateauing (see figure8). Black line indicate slope 0.5.

In order to extract a general behaviour from these different observations, we focused on $\frac{\Delta P_{min}}{\Delta P_{Landau}}$, the minimum value of $\frac{\Delta P}{\Delta P_{Landau}}$ after buckling - this can indeed be considered as the plateauing value for $\frac{d}{R} > 0.014$. Data obtained for $\nu = 0.5$ can be compared with results published in [11] ; the use of curvature energy given by equation (6) makes them differ from less than 20%. Figure 9 shows that power-laws of the type $\frac{\Delta P_{min}}{\Delta P_{Landau}} = a(\nu) \times \left(\frac{d}{R}\right)^{0.5}$ are to be found in the plateauing regime. Similarly to what was done in section 3, and since $a(\nu)$ appears to be even (curves at $\nu = 0.5$ and $\nu = -0.5$ mix up on figure 9), we searched it under the form $(1 - \nu^2)^x$, minimizing x for the best fits at $\frac{d}{R} > 0.014$. This led us to propose the master curve presented on figure 9, of formula $\frac{\Delta P_{min}}{Y_{3D}} \times (1 - \nu^2)^{0.773} = 0.75 \times \left(\frac{d}{R}\right)^{2.5}$. We do not have for the moment theoretical clues to justify these two successive fitting operations, but it provides reduced values that impressively gather on a single curve, for γ ranging from $8 \cdot 10^2$ to $4.7 \cdot 10^5$, and for ν between -0.8 and 0.5. This result, exposed on figure 10 with 3D parameters, is expected to be of practical use for all experiments involving deflation controlled by the volume. On a more conceptual point of view, plot clearly confirms two different scalings of the pressure during deflation, around a threshold in relative thickness $\left(\frac{d}{R}\right)_c \approx 0.013$. This may be an indication of the existence of different ways to accommodate s-cones on a sphere, and requires further investigations.

6 Conclusion

Systematic numerical study of the buckling of a spherical shell, in the conformation with a single depression, allows to sketch the influence of the different geometrical or elastic parameters through quite simple phenomenological laws. The surface model can be translated in 3D parameters, that are the shell's thickness, and the two elastic parameters of the material that compose it: Young modulus and Poisson's ratio.

At imposed volume, the Young modulus does not play on the shape. Results showed that the first transition (toward axysymmetrically buckled shape), and the second one, with appearance of wrinkles, or "s-cones", is mainly driven by $\frac{d}{R}$ for non-auxetic (*i.e.* with positive Poisson's ratio) materials. For auxetic materials, the Poisson's ratio may have a determining importance, by strongly displacing transitions toward higher values of the relative volume variation, up to possible vanishing. Decreasing the Poisson's

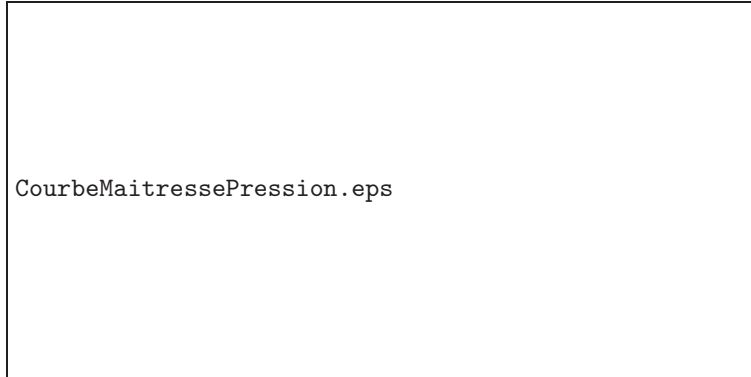


Figure 10: Pressure master curve after first buckling: $\frac{\Delta P_{min}}{Y_{3D}} \times (1 - \nu^2)^{0.773}$ versus $\frac{d}{R}$. Black squares: $\nu = 0.5$; black diamonds: $\nu = 0$; light grey diamonds: $\nu = -0.5$; white diamonds: $\nu = -0.8$. Continuous line: $\frac{\Delta P_{min}}{Y_{3D}} \times (1 - \nu^2)^{0.773} = 0.75 \times \left(\frac{d}{R}\right)^{2.5}$.

ratio down to very negative values stabilizes spherical deflation at the expense of dimples creation, and axisymmetric dimples against appearance of wrinkles.

The number of wrinkles indicate a dependence in $\left(\frac{d}{R}\right)^{-1/2}$, that confirms \sqrt{dR} as the accurate scaling for elastic deformations of elastic spherical surfaces.

The Young modulus scales pressure features: critical inside/outside pressure difference that triggers first buckling, and plateauing pressure after buckling. Detailed behaviour, that is shown to reduce to a master curve, opens the possibility for two different wrinkling regimes.

Acknowledgments

The author thanks K. Brakke for developing and maintaining the Surface Evolver software, including invaluable interactions during this work, and P. Marmottant and F. Quéméneur for fruitful discussions.

References

- [1] A. V. Pogorelov, *Bending of surfaces and stability of shells* (American Mathematical Society, Providence, 1988)
- [2] L. Landau, E. M. Lifschitz, *Theory of elasticity*, 3rd ed., Elsevier Butterworth-Heinemann, Oxford 1986
- [3] R. L. Carlson, R. L. Sendelbeck, N. J. Hoff, *Exp. Mech.* 7, 281 (1967)
- [4] N. Tsapis, E. R. Dufresne, S. S. Sinha, C. S. Riera, J. W. Hutchinson, L. Mahadevan, D. A. Weitz, *Phys. Rev. Lett.* 94, 018302 (2005)
- [5] C. I. Zoldesi, A. I. Imhof, *Adv. Mat.* 17, 924 (2005)
- [6] S.S. Datta, H. C. Shum, D. A. Weitz, *Langmuir* 26, 18612 (2010)

- [7] D. Sen, J.S. Melo, J. Bahadur, S. Mazumder, S. Bhattacharya, G. Gosh, D. Dutta, S.F. D'Souza, Eur. Phys. J. B 31, 393 (2010)
- [8] S. Sacanna, W. T. M. Irvine, L. Rossi, D. J. Pine, Soft Matter 7, 1631 (2011)
- [9] G. A. Vliegenthart, G. Gompper, New J. Phys. 13, 045020 (2011)
- [10] M. Okubo, H. Minami, K. Morikawa, Colloid Polym. Sci. 279, 931 (2001)
- [11] C. Quilliet, C. Zoldesi, C. Riera, A. van Blaaderen, A. Imhof, Eur. Phys. J. E 27, 13 (2008) and erratum 32, 419 (2010)
- [12] L. Pauchard, S. Rica, Phil. Mag. B 78, 225 (1998)
- [13] A. Vaziri, Thin-Walled Struct. 47, 692 (2009)
- [14] S. Komura, K. Tamura, T. Kato, Eur. J. Phys. E 18, 343 (2005)
- [15] F. Quéméneur, C. Quilliet, M. Faivre, A. Viallat, B. Pépin-Donat, submitted
- [16] Calculations of ref. C. Quilliet, Phys. Rev. E 74, 046608 (2006) led to the inverse conclusion. With current hindsight, it appears that the elastic energy of dimples of important size (approaching the shell's one) was overestimated in this paper. In the pure curvature model used in it, following ref. [25] the rim's curvature was estimated as $\sqrt{Rd}/\tan\alpha$, where α is the half-angle of the cone in which the dimples inscribes ; this term caused quick increase of the elastic energy with α . More recent calculations showed that lateral extension of the rim is better described by \sqrt{Rd}/α before autocontact [23] ; this prevents multiple indentation to be of lower energy than single indentation in the pure curvature model.
- [17] B. Audoly, Y. Pomeau, *Elasticity and Geometry: From hair curls to the nonlinear response of shells*, Oxford Univ. Press, 2010
- [18] W. Helfrich, Z. Naturforsch. C28, 693 (1973)
- [19] There may be discrepancies between different communities about the definitions of both κ and c . Here we used definitions that rule in the Soft Matter community, and more particularly in physics of lipids vesicles: $c = \frac{1}{R_1} + \frac{1}{R_2}$, where R_1 and R_2 are the main algebraic curvature radii (mathematicians usually consider half of this quantity). And we take κ such that the bending energy of a sphere is $8\pi\kappa$.
- [20] P. Marmottant, A. Bouakaz, N. De Jong, C. Quilliet, J. Acoust. Soc. Am. 129, 1231 (2011)
- [21] P. Marmottant, A. Farutin, C. Quilliet, C. Misbah, submitted
- [22] J. Lidmar, L. Mirny, D. R. Nelson, Phys. Rev. E 68, 051910 (2003)
- [23] S. Knoche and J. Kierfeld, arXiv:1108.3487v1.
- [24] K. Brakke, Exp. Math. 1, 141 (1992)
- [25] L. Pauchard, Y. Pomeau, S. Rica, C. R. A. S. Iib 323, 411 (1997)
- [26] S. Chaïeb, F. Melo, J.-C. Géminard, Phys. Rev. Lett. 80, 2354 (1998)
- [27] E. Cerda, L. Mahadevan, Proc. Royal Soc. A, 461, 671 (2005)
- [28] A. Lazarus and P. Reis, private communication